
AGARD

ADVISORY GROUP FOR AEROSPACE RESEARCH & DEVELOPMENT

7 RUE ANCELLE 92200 NEUILLY SUR SEINE FRANCE

PROPAGATION MODELING OF MOIST AIR AND SUSPENDED
WATER/ICE PARTICLES AT FREQUENCIES BELOW 1000 GHz

H. J. Liebe
G. A. Hufford
M. G. Cotton

National Telecommunications and Information Administration
Institute for Telecommunication Sciences
325 Broadway, Boulder, CO 80303
U.S.A

**Paper Reprinted from
AGARD Conference Proceedings 542**

Atmospheric Propagation Effects through Natural and Man-Made Obscurants for Visible to MM-Wave Radiation

(Les Effets des Conditions Défavorables de
Propagation sur les Systèmes Optiques,
IR et à Ondes Millimétriques)

*Presented at the Electromagnetic Wave Propagation Panel Symposium,
held in Palma de Mallorca, Spain, 17th—20th May 1993.*



NORTH ATLANTIC TREATY ORGANIZATION

The Mission of AGARD

According to its Charter, the mission of AGARD is to bring together the leading personalities of the NATO nations in the fields of science and technology relating to aerospace for the following purposes:

- Recommending effective ways for the member nations to use their research and development capabilities for the common benefit of the NATO community;
- Providing scientific and technical advice and assistance to the Military Committee in the field of aerospace research and development (with particular regard to its military application);
- Continuously stimulating advances in the aerospace sciences relevant to strengthening the common defence posture;
- Improving the co-operation among member nations in aerospace research and development;
- Exchange of scientific and technical information;
- Providing assistance to member nations for the purpose of increasing their scientific and technical potential;
- Rendering scientific and technical assistance, as requested, to other NATO bodies and to member nations in connection with research and development problems in the aerospace field.

The highest authority within AGARD is the National Delegates Board consisting of officially appointed senior representatives from each member nation. The mission of AGARD is carried out through the Panels which are composed of experts appointed by the National Delegates, the Consultant and Exchange Programme and the Aerospace Applications Studies Programme. The results of AGARD work are reported to the member nations and the NATO Authorities through the AGARD series of publications of which this is one.

Participation in AGARD activities is by invitation only and is normally limited to citizens of the NATO nations.

REPORT DOCUMENTATION PAGE			
1. Recipient's Reference	2. Originator's Reference	3. Further Reference	4. Security Classification of Document
	AGARD-CP-542	ISBN 92-835-0727-4	UNCLASSIFIED/ UNLIMITED
5. Originator	Advisory Group for Aerospace Research and Development North Atlantic Treaty Organization 7 Rue Ancoele, 92200 Neuilly sur Seine, France		
6. Title	ATMOSPHERIC PROPAGATION EFFECTS THROUGH NATURAL AND MAN-MADE OBSCURANTS FOR VISIBLE TO MM-WAVE RADIATION		
7. Presented at	the Electromagnetic Wave Propagation Panel Symposium, held in Palma de Mallorca, Spain, 17th-20th May 1993.		
8. Author(s)/Editor(s)	Various		9. Date November 1993
10. Author's/Editor's Address	Various		11. Pages 208

14. Abstract
This publication reports the papers presented to a specialists' meeting held by the Electromagnetic Wave Propagation Panel at its Spring 1993 meeting.
The topics covered on the occasion of that Symposium include:
Natural obscurants:
— The effects of natural obscurants (haze, clouds, fog, rain, snow and dust) on system performance.
Man-made obscurants and battlefield-induced phenomena:
— The effects of man-made smokes, battlefield-induced smokes and enhanced scintillation on system performance.
Target and background signatures:
— Atmospheric effects on target and background signatures, and target to background contrast.
Multispectral camouflage:
— Weather-related propagation effects on camouflage and obscurants effectiveness and contrast reduction.
— Theoretical and/or experimental evaluation of camouflage effectiveness.
System mitigation aspects:
— Methods to mitigate the above-mentioned factors e.g. image processing, sensor fusion, tactical weather intelligence, and tactical decision aids.

Published November 1993

Copyright © AGARD 1993

All Rights Reserved

ISBN 92-835-0727-4



Printed by Specialised Printing Services Limited
40 Chigwell Lane, Loughton, Essex IG10 3TZ

**PROPAGATION MODELING OF MOIST AIR AND SUSPENDED
WATER/ICE PARTICLES AT FREQUENCIES BELOW 1000 GHz**

H. J. Liebe
G. A. Hufford
M. G. Cotton

National Telecommunications and Information Administration
Institute for Telecommunication Sciences
325 Broadway, Boulder, CO 80303
U.S.A

SUMMARY

Propagation characteristics of the atmosphere are modeled for the frequency range from 1 to 1000 GHz (1 THz) by the modular millimeter-wave propagation model MPM. Refractivity spectra of the main natural absorbers (i.e., oxygen, water-vapor, suspended droplets and ice particles) are computed from known meteorological variables. The primary contributions of dry air come from 44 O₂ lines. Results from extensive 60-GHz laboratory measurements of the pressure-broadened O₂ spectrum were applied to update the line data base. The water-vapor module considers 34 local H₂O lines plus continuum contributions from the H₂O spectrum above 1 THz, which are formulated as wing response of a pseudo-line centered at 1.8 THz. Cloud/fog effects are treated with the Rayleigh approximation employing revised formulations for the permittivities of water and ice.

The influence of the Earth's magnetic field on O₂ absorption lines becomes noticeable at altitudes between 30 and 120 km. Anisotropic medium properties result, which are computed by the Zeeman propagation model ZPM. Here the elements of a complex refractivity tensor are determined in the vicinity (± 10 MHz) of O₂ line centers and their effect on the propagation of plane, polarized radiowaves is evaluated.

A spherically stratified (0 - 130 km) atmosphere provides the input for the codes MPM and ZPM in order to analyze transmission and emission properties of radio paths. Height profiles of air and water vapor densities and of the geocoded magnetic field are specified. ZPM predicts polarization- and direction-dependent propagation through the mesosphere. Emission spectra of the 9⁺ line (61150 \pm 3 MHz) for paths with tangential heights ranging from 30 to 125 km are consistent with data measured by the shuttle-based millimeter-wave limb sounder MAS.

1. INTRODUCTION

The natural atmospheric absorbers of oxygen, water vapor, and suspended water-droplets or ice-crystals, determine the propagation properties of the nonprecipitating atmosphere. The spectral characteristics of these absorbers are predicted up to 1000 GHz based on the physical conditions at altitudes from sea level to 130 km. Both phase and amplitude response of a plane radio wave propagating the distance z at frequency ν are described by a field strength,

$$E(z) = \exp[i k z (1 + N \times 10^{-6})] E(0),$$

where $E(0)$ is the initial value, $k = 2\pi\nu/c$ is the free space wave number, and c is the speed of light in vacuum. The spectral characteristics of the atmospheric medium are

expressed by a complex refractivity,

$$N = N_0 + N' + i N'' \quad \text{ppm} \quad (1)$$

The real part changes the propagation velocity (refraction) and consists of a frequency-independent term, N_0 , plus the dispersive refraction $N'(\nu)$. The imaginary part quantifies the loss of radiation energy (absorption). Refractivity N determines the specific quantities of power attenuation α and phase dispersion β or delay rate τ . Assuming frequency ν in GHz, one obtains

$$\begin{aligned} \alpha &= 0.1820 \nu N'' && \text{dB/km,} \\ \beta &= 1.2008 \nu (N_0 + N') && \text{deg/km,} \\ \tau &= 3.3356 (N_0 + N') && \text{ps/km.} \end{aligned}$$

Under special circumstances the refractivity N can exhibit *anisotropic* properties (e.g., mesospheric O₂ Zeeman effect). In such a case the propagation of plane, polarized waves is characterized by a two-dimensional field vector $E^*(z)$ which is affected perpendicular to the direction of propagation by a 2×2 refractivity matrix N .

2. ATMOSPHERIC REFRACTIVITY

2.1 Input Variables

Complex refractivity N is the central quantity computed by the Millimeter-wave Propagation Model MPM.^{1,2} Here, the opportunity is taken to update MPM89² with the latest spectroscopic information. The model considers 44 O₂ and 34 H₂O local lines (centered below 1000 GHz), nonresonant spectra for dry air, and an empirical water vapor continuum which reconciles experimental discrepancies. Model formulations for dry air and water vapor spectra follow closely the theory of absorption by atmospheric gases that is reviewed in detail by Rosenkranz.³ The refractivity of suspended water and ice particles is computed with the Rayleigh absorption approximation.⁴ Atmospheric conditions in MPM are characterized by the input variables:

		Typical Range
- barometric pressure	p	10^5 - 1013 mb
- ambient temperature	t	-100 - 50 °C
- relative humidity	u	0 - 100 %
- water droplet density	w	0 - 5 g/m ³
- ice particle density	w_i	0 - 1 g/m ³
- magnetic field strength	B	20 - 65 μ T.

For modeling purposes, a reciprocal temperature variable is introduced, $\theta = 300/(t + 273.15)$, and the barometric pressure p (1 mb = 100 Pa) is separated into partial pressures for dry air (p_d) and water vapor (e); i.e.,

$$p = p_d + e \quad \text{mb.}$$

2.2 Dry-Air Module

Refractivity of dry air is expressed by

$$N_D = N_d + \sum_k S_k F_k + N_n \quad \text{ppm}, \quad (2)$$

where the nondispersive term is

$$N_d = 0.2588 p_d \theta.$$

2.2.1 Oxygen Line Terms

The main contributions to N_D come from 44 O_2 spectral lines ($k =$ line index). Each line strength,

$$S_k = (a_1 / \nu_k) p_d \theta^3 \exp [a_2 (1 - \theta)] \quad \text{ppm},$$

is multiplied by the complex shape function,

$$F(\nu) = \nu \left[\frac{1 - i\delta_k}{\nu_k - \nu - i\gamma_k} - \frac{1 + i\delta_k}{\nu_k + \nu + i\gamma_k} \right] \quad (3)$$

The Van Vleck-Weisskopf function $F(\nu)$ was modified by Rosenkranz³ to include line overlap effects. Width (γ) and overlap (δ) parameters of pressure-broadened O_2 lines in air are

$$\gamma_k = a_3 \times 10^{-3} (p_d \theta^{2.4} + 1.10 e \theta) \quad \text{GHz}$$

and

$$\delta_k = (a_5 + a_6 \theta) p \theta^{0.8}.$$

A rough estimate of line behavior in the mesosphere can be obtained by replacing γ_k with

$$\gamma_h = (\gamma_k^2 + 625 B^2)^{1/2},$$

where B is the magnetic field strength (22 - 65 μT) depending on the geographic location and altitude (see Sect. 2.3).

Extensive laboratory measurements of 60-GHz absorption by dry air have been reported recently.⁵ A best fit to these data established new coefficients a_5 and a_6 for the microwave lines. Still, the values listed for a_3 and $a_{5,6}$ in Table 1 are different from Ref. 5. Indirect evidence from the data suggests that all microwave widths γ_k are multiplied by 1.05.

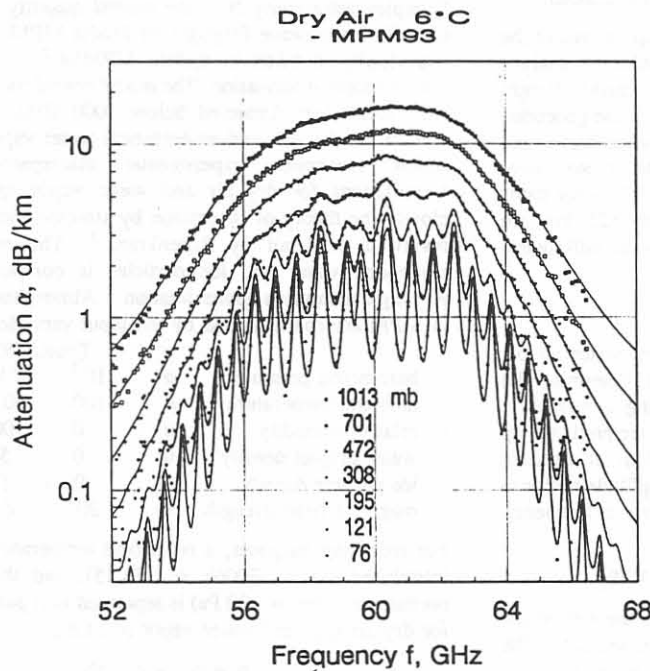


Figure 1. Dry air attenuation α from 52 to 68 GHz at 6°C for pressures from 1013 to 76 mb: MPM93 (lines), measured data⁵ (symbols).

This correction reduced on the average by 7 percent the rms error of the residuals for all 5400 data points when, in addition, the δ_k 's were raised by a factor of 1.15.⁵ Center frequencies ν_k and spectroscopic coefficients a_1 to a_6 are listed in Table 1.

The good fit between predicted attenuation rates and measured data points is illustrated in Fig. 1. Some of the very first attenuation rates (14 values, 49 - 59 GHz) for sea-level conditions were reported in 1956.⁶ These field-measured data agree well with predictions based on Eq. (2).

2.2.2 Nonresonant Terms

Nonresonant refractivity,

$$N_n = S_o F_o(\nu) + i S_n F_n''(\nu) \quad \text{ppm},$$

consists (a) of the nonresonant O_2 spectrum,

$$S_o = 6.14 \times 10^{-5} p_d \theta^2,$$

$$F_o = -\nu / (\nu + i\gamma_o),$$

where the relaxation frequency is $\gamma_o = 0.56 \times 10^{-3} p \theta^{0.8}$; and (b) of small contributions above 100 GHz by pressure-induced N_2 absorption,

$$S_n = 1.40 \times 10^{-12} p_d^2 \theta^{3.5},$$

$$F_n'' = \nu / (1 + 1.9 \times 10^{-5} \nu^{1.5}).$$

2.3 Zeeman-Effect of O_2 Lines

In the mesosphere, oxygen line absorption is complicated.⁷⁻⁹ Three separate complex-valued Zeeman refractivity patterns, $N_{\sigma+}$ and $N_{\sigma-}$, are brought out by the geomagnetic field vector B^* . The refractivity that influences the field components of a plane wave is expressed in matrix form,⁸

$$N = \begin{bmatrix} N_{\sigma+} \sin^2 \phi + (N_{\sigma+} + N_{\sigma-}) \cos^2 \phi & -i(N_{\sigma+} - N_{\sigma-}) \cos \phi \\ i(N_{\sigma+} + N_{\sigma-}) \cos \phi & N_{\sigma+} + N_{\sigma-} \end{bmatrix}$$

where ϕ is the angle between the direction of propagation and the magnetic vector B^* . The refractivity elements of an isolated line are represented by

$$N_{\sigma\pm, \tau} = N_d + S_k \sum_M \xi_M F_M \quad \text{ppm}, \quad (4)$$

where ξ_M is a relative strength factor defined in such a way that the sum of the Zeeman components equals the strength value (a_1) of the unsplit ($B = 0$) line. The center frequency of individual lines within a pattern is determined by

$$\nu_M = \nu_k + 28.03 \times 10^{-6} \eta_M B \quad \text{GHz},$$

where the relative shift factor η_M lies between +1 and -1. The index M stands for the azimuthal quantum number M , which controls the structure of a Zeeman pattern.⁹ The scheme for determining ξ_M and η_M hinges on the quantum number identification of a particular O_2 line and can be found in Refs. 8, 9. The correct shape function is a Voigt profile,³ which was approximated by a Lorentzian profile,

$$F_M = \nu / (\nu_M - \nu - i\gamma_h),$$

where the transition to Doppler-broadening at $h \geq 50$ km ($p \leq 0.8$ mb) is given for each Zeeman component by

$$\gamma_h = 0.535 \gamma_k + (0.217 \gamma_k^2 + \gamma_D^2)^{1/2} \quad \text{GHz}.$$

The Doppler width is $\gamma_D = 1.096 \times 10^{-6} \nu_M \theta^{1/2}$.

2.4 Water-Vapor Module

The MPM-input for water vapor is relative humidity u , which is converted to vapor pressure $e = (u/100) e_s$ by way of the saturation pressure e_s over water (or ice)¹⁰ at temperature t . A useful approximation for saturation over water is given by

$$e_s = 2.408 \times 10^{11} \theta^{5.5} \exp(-22.644 \theta) \text{ mb.}$$

Absolute humidity (water-vapor density) follows from

$$q = 0.7223 e \theta \text{ g/m}^3.$$

Refractivity of atmospheric water vapor is written in the form

$$N_V = N_V + \sum_t S_t F_t + N_c \text{ ppm,} \quad (5)$$

where the nondispersive term is

$$N_V = (4.163 \theta + 0.239) e \theta.$$

2.4.1 H₂O Line Spectrum

Line refractivity results from 34 local H₂O resonances (ℓ = line index). The individual line strength is

$$S_\ell = (b_1 / \nu_\ell) e \theta^{3.5} \exp[b_2(1 - \theta)] \text{ ppm;}$$

the shape function is that of Eq. (3). The width of a pressure-broadened H₂O line is formulated by¹¹

$$\gamma_\ell = b_3 \times 10^{-3} (b_4 e \theta^{b_6} + p_d \theta^{b_5}) \text{ GHz.}$$

Line overlap is neglected ($\delta_\ell = 0$) and Doppler-broadening is approximated for pressures below 0.7 mb ($h \geq 60$ km) by

$$\gamma_\ell^* = 0.535 \gamma_\ell + (0.217 \gamma_\ell^2 + \gamma_D^2)^{1/2},$$

where the Doppler width is $\gamma_D = 1.46 \times 10^{-6} \nu_\ell \theta^{-1/2}$.

2.4.2 H₂O Continuum Spectrum

The contributions of local lines in Eq. (5) are not sufficient to match measured data. In particular, absorption data in the window ranges between spectral lines reflect a magnitude up to five times larger than predicted values. The excess is taken into account by a continuum spectrum N_c , which originates in the strong lines centered in the rotational H₂O spectrum above 1 THz.^{14, 20} Absolute absorption data from controlled experiments^{15 - 19} provide the basis for formulating a physical model of N_c . Pure water vapor and foreign-gas (air or N₂) mixtures were studied at 18 - 40 GHz¹⁵, 138 GHz¹⁶, 186 - 194 GHz¹⁷, 213.5 GHz¹⁸, and 160 - 920 GHz¹⁹.

At 137.8 GHz, pressure and temperature dependences of moist air absorption data were fitted with 10% rms to¹⁶

$$N_c = e (k_s e + k_f p_d) 10^{-6} \nu \text{ ppm,} \quad (6)$$

where $k_s = 0.357 \theta^{7.5}$ and $k_f = 0.0113 \theta^3$. This equation was then applied to define the continuum for MPM89.²

At 213.5 GHz, new absorption data of moist nitrogen have been reported,¹⁸ which fitted with an oxygen-free MPM exceptionally well to Eq. (6):

$$k_s = 0.444 \theta^{7.5} \quad (0.4\% \text{ rms}) \text{ and}$$

$$k_f = 0.0145 \theta^{4.5} \quad (1.0\% \text{ rms}).$$

Similar data closer to the 183-GHz line center¹⁷ yielded initially a fitting error of 14.6% rms, which improved to 4.5% rms when the theoretical¹² strength value b_1 was increased by 5 percent. A theoretical approximation of the real part,²⁰

$$N_c' = e \theta^{2.5} 0.791 \times 10^{-6} \nu^2 \text{ ppm,}$$

was also considered in the fitting exercise.

An analytical match of the continuum was considered by means of a *pseudo*-line centered out-of-band above 1 THz. Expanding the line shape, Eq. (3), into a power series and assuming that $\delta = 0$, $\gamma_c \ll \nu_c$, and $\nu \rightarrow 0$, leads to:

$$N_c'' \approx 2 S_c \gamma_c [(\nu/\nu_c) + 3 (\nu/\nu_c)^3] \nu_c^{-2} \text{ and} \quad (7)$$

$$N_c' \approx 2 S_c [(\nu/\nu_c)^2 + (\nu/\nu_c)^4] \nu_c^{-1}$$

Different fits to Eq. (7) resulted in three sets of parameters for this pseudo-line:

ν_c	b_1	b_2	b_3	b_4	b_5	b_6	Data Ref.
GHz	kHz/mb		MHz/mb				
2200	4210	0.952	17.8	30.5	2	5	15, 18, 19
1780	2230	0.952	17.6	30.5	2	5	15, 18, Table 2
1470	1257	0.952	17.3	30.5	2	5	15, 18, 20

For the "continuum" line N_c centered at $\nu_c = 1780$ GHz and the chosen units one can assert that

$$k_s (\theta = 1) = 2 \times 10^3 b_1 b_3 b_4 \nu_c^{-3} = 0.434 \text{ GHz}^{-1} \text{ mb}^{-2},$$

which is close to the value found by fitting the 213.5-GHz data alone (see above). The second-order ν -terms of Eq. (7) allow one to "tailor" the fit close to the upper frequency limit of MPM (1 THz) by changing ν_c . An exact fit to both measured absorption data¹⁹ and analytical refraction results²⁰ around 900 GHz was not possible. Hence, the continuum line parameters ν_c and b_1 in Table 2 are a compromise which is of no consequence to data fits below about 800 GHz. Both the large widths for far-wing self- $(b_3 \times b_4)$ and air-broadening (b_3) and the strong negative temperature dependence (b_6) have been postulated by theory.^{14, 21}

Table 2 lists the present line frequencies ν_ℓ and spectroscopic coefficients b_1 to b_6 (ν_ℓ and b_1 are from Ref. 12). The b_1 values of the 22-GHz line* and 183-GHz¹⁷ lines were increased by 5 percent to fit measured data.

The MPM for moist air is made up by $N = N_D + N_V$. Predictions of N'' are compared with published data in Figs. 2 to 4. The critical temperature dependence of N_c'' is represented in Fig. 2. The frequency dependence of three data sets^{15, 17-19} is shown in Figs. 3 and 4. Measured data in Fig. 4 span a range from 160 to 920 GHz.¹⁹ MPM-predicted attenuation rates $\alpha(\nu)$ are plotted in Fig. 5 for sea-level conditions (100% RH) at five temperatures ($\pm 40^\circ\text{C}$).

2.5 Cloud/Fog Module

The interaction of suspended water droplets and ice crystals with radio waves is treated by employing the Rayleigh approximation for Mie extinction,

$$N_W = 1.5 (w/m_{w,i}) [(\epsilon_{w,i} - 1)(\epsilon_{w,i} + 2)^{-1}], \quad (8)$$

where $m_{w,i} = 1$ and $0.916 \text{ (g/cm}^3\text{)}$ are specific weights, and $\epsilon_{w,i}$ complex permittivities of water and ice, respectively.⁴ For the size spectra ($r \leq 50 \mu\text{m}$) of suspended water droplets, Eq. (8) is valid up to about 300 GHz. Fog or cloud conditions are specified by a water mass density w . Water droplets form when the relative humidity exceeds saturation, $u = 100 - 101$ percent, whereby t can be as low as -40°C (supercooled state). Propagation effects caused by ice crystals (needles and plates) are primarily depolarizing and scattering in nature.

* The increase in the b_1 -coefficient for the 22.2-GHz line was suggested by ground-level emission measurements.¹³ Data at 20.6 GHz exhibited a systematic trend which was not apparent in 31.7- and 90-GHz data taken simultaneously. On-site radiosonde recordings of height profiles for p , t , and u furnished independent input to test three prediction models.

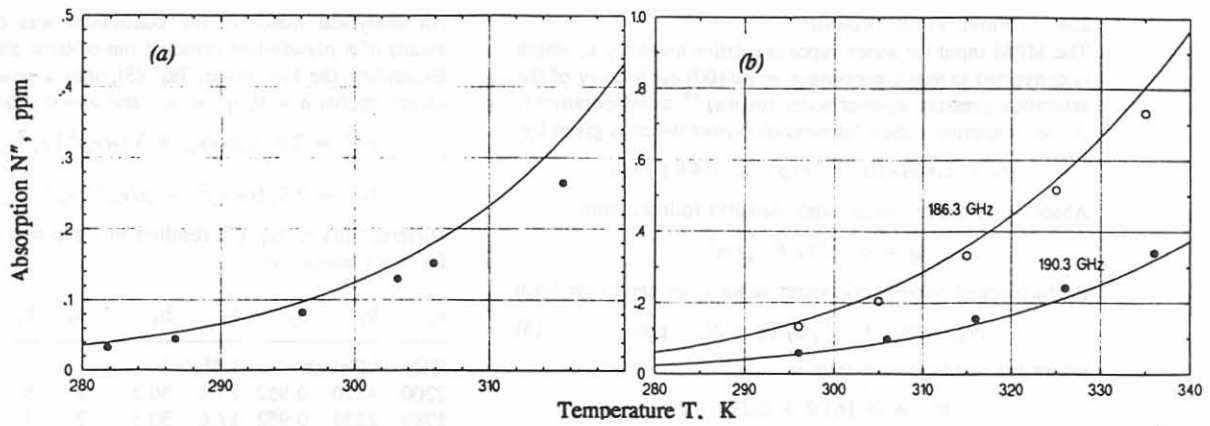


Figure 2. Absorption data N'' versus temperature T in kelvin: (a) moist air at 137.8 GHz ($p = 1013$ mb, $u = 80\%$)¹⁶, and (b) mixture of water vapor and nitrogen (186.3 and 190.3 GHz, $p = 1000$ mb, $u = 10\%$)¹⁷. — MPM93.

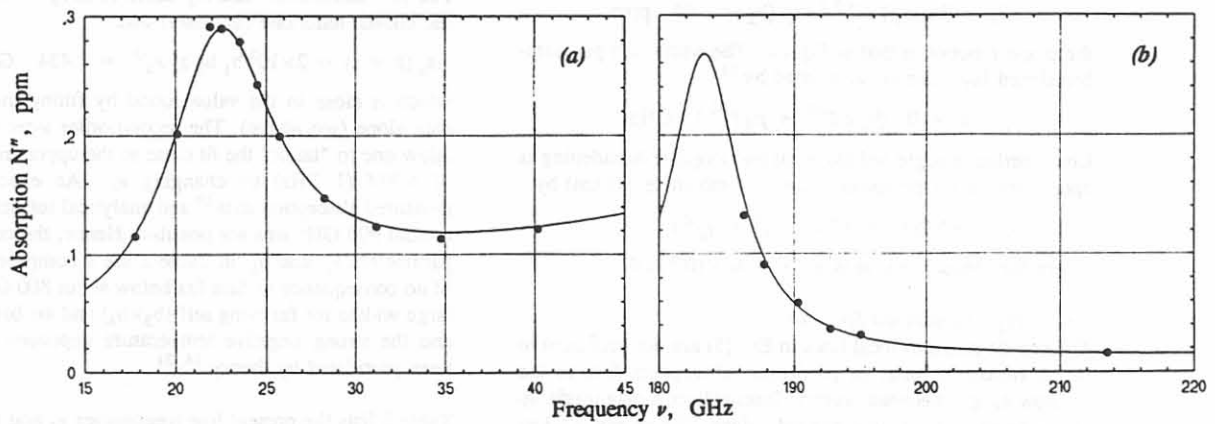


Figure 3. Absorption data N'' over two frequency ranges: (a) moist air (318 K, $p = 1013$ mb, $u = 80\%$)¹⁵, and (b) mixture of water vapor and nitrogen (296 K, $p = 1000$ mb, $u = 10\%$)^{17, 18}. — MPM93.

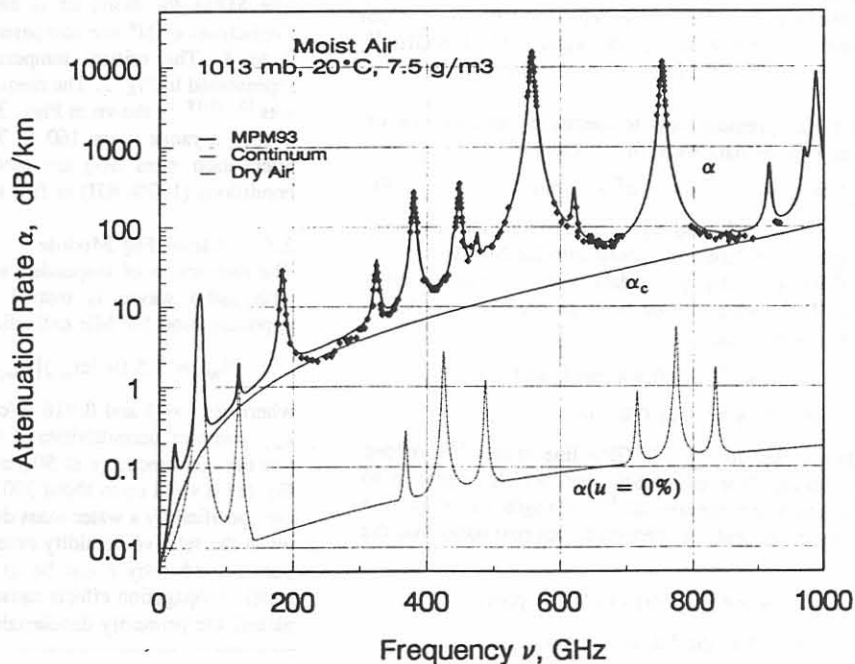


Figure 4. Attenuation rate α and continuum of moist air ($u = 43.4\%$) and of dry air ($u = 0\%$) as predicted by MPM93 for standard sea-level conditions ($p = 1013$ mb, $t = 20^\circ\text{C}$). Data points are from Ref. 19.

TABLE 1. Spectroscopic Coefficients of O₂ Lines in Air

Center Freq. ν_k	Strength		Width		Overlap	
	a_1	a_2	a_3^*	a_4	a_5^*	a_6^*
GHz	kHz/mb		MHz/mb		10^3 /mb	
50.474238	9.400E-08	9.694	0.89	0.8	0.240	0.790
50.987749	2.460E-07	8.694	0.91	0.8	0.220	0.780
51.503350	6.080E-07	7.744	0.94	0.8	0.197	0.774
52.021410	1.414E-06	6.844	0.97	0.8	0.166	0.764
52.542394	3.102E-06	6.004	0.99	0.8	0.136	0.751
53.066907	6.410E-06	5.224	1.02	0.8	0.131	0.714
53.595749	1.247E-05	4.484	1.05	0.8	0.230	0.584
54.130000	2.280E-05	3.814	1.07	0.8	0.335	0.431
54.671159	3.918E-05	3.194	1.10	0.8	0.374	0.305
55.221367	6.316E-05	2.624	1.13	0.8	0.258	0.339
55.783802	9.535E-05	2.119	1.17	0.8	-0.166	0.705
56.264775	5.489E-05	0.015	1.73	0.8	0.390	-0.113
56.363389	1.344E-04	1.660	1.20	0.8	-0.297	0.753
56.968206	1.763E-04	1.260	1.24	0.8	-0.416	0.742
57.612484	2.141E-04	0.915	1.28	0.8	-0.613	0.697
58.323877	2.386E-04	0.626	1.33	0.8	-0.205	0.051
58.446590	1.457E-04	0.084	1.52	0.8	0.748	-0.146
59.164207	2.404E-04	0.391	1.39	0.8	-0.722	0.266
59.590983	2.112E-04	0.212	1.43	0.8	0.765	-0.090
60.306061	2.124E-04	0.212	1.45	0.8	-0.705	0.081
60.434776	2.461E-04	0.391	1.36	0.8	0.697	-0.324
61.150560	2.504E-04	0.626	1.31	0.8	0.104	-0.067
61.800154	2.298E-04	0.915	1.27	0.8	0.570	-0.761
62.411215	1.933E-04	1.260	1.23	0.8	0.360	-0.777
62.486260	1.517E-04	0.083	1.54	0.8	-0.498	0.097
62.997977	1.503E-04	1.665	1.20	0.8	0.239	-0.768
63.568518	1.087E-04	2.115	1.17	0.8	0.108	-0.706
64.127767	7.335E-05	2.620	1.13	0.8	-0.311	-0.332
64.678903	4.635E-05	3.195	1.10	0.8	-0.421	-0.298
65.224071	2.748E-05	3.815	1.07	0.8	-0.375	-0.423
65.764772	1.530E-05	4.485	1.05	0.8	-0.267	-0.575
66.302091	8.009E-06	5.225	1.02	0.8	-0.168	-0.700
66.836830	3.946E-06	6.005	0.99	0.8	-0.169	-0.735
67.369598	1.832E-06	6.845	0.97	0.8	-0.200	-0.744
67.900867	8.010E-07	7.745	0.94	0.8	-0.228	-0.753
68.431005	3.300E-07	8.695	0.92	0.8	-0.240	-0.760
68.960311	1.280E-07	9.695	0.90	0.8	-0.250	-0.765
118.750343	9.450E-05	0.009	1.63	0.8	-0.036	0.009
368.498350	6.790E-06	0.049	1.92	0.2	0	0
424.763124	6.380E-05	0.044	1.93	0.2	0	0
487.249370	2.350E-05	0.049	1.92	0.2	0	0
715.393150	9.960E-06	0.145	1.81	0.2	0	0
773.839675	6.710E-05	0.130	1.82	0.2	0	0
834.145330	1.800E-05	0.147	1.81	0.2	0	0

TABLE 2. Spectroscopic Coefficients of H₂O Lines in Air

Center Freq. ν_l	Strength		Width			
	b_1^*	b_2	b_3	b_4	b_5	b_6
GHz	kHz/mb		MHz/mb			
22.235080	0.01130 ⁺	2.143	2.811	4.80	0.69	1.00
67.803960	0.00012	8.735	2.858	4.93	0.69	0.82
119.995940	0.00008	8.356	2.948	4.78	0.70	0.79
183.310091	0.24200 ⁺	0.668	3.050 ⁺	5.30	0.64	0.85
321.225644	0.00483	6.181	2.303	4.69	0.67	0.54
325.152919	0.14990	1.540	2.783	4.85	0.68	0.74
336.222601	0.00011	9.829	2.693	4.74	0.69	0.61
380.197372	1.15200	1.048	2.873	5.38	0.54 ⁺	0.89 ⁺
390.134508	0.00046	7.350	2.152	4.81	0.63	0.55
437.346667	0.00650	5.050	1.845	4.23	0.60	0.48
439.150812	0.09218	3.596	2.100	4.29	0.63	0.52
443.018295	0.01976	5.050	1.860	4.23	0.60	0.50
448.001075	1.03200	1.405	2.632	4.84	0.66	0.67
470.888947	0.03297	3.599	2.152	4.57	0.66	0.65
474.689127	0.12620	2.381	2.355	4.65	0.65	0.64
488.491133	0.02520	2.853	2.602	5.04	0.69	0.72
503.568532	0.00390	6.733	1.612	3.98	0.61	0.43
504.482692	0.00130	6.733	1.612	4.01	0.61	0.45
547.676440*	0.97010	0.114	2.600	4.50	0.70	1.00
552.020960*	1.47700	0.114	2.600	4.50	0.70	1.00
556.936002	48.74000	0.159	3.210	4.11	0.69	1.00
620.700807	0.50120	2.200	2.438	4.68	0.71	0.68
645.866155*	0.00713	8.580	1.800	4.00	0.60	0.50
658.005280	0.03022	7.820	3.210	4.14	0.69	1.00
752.033227	23.96000	0.396	3.060	4.09	0.68	0.84
841.053973	0.00140	8.180	1.590	5.76	0.33	0.45
859.962313	0.01472	7.989	3.060	4.09	0.68	0.84
899.306675	0.00605	7.917	2.985	4.53	0.68	0.90
902.616173	0.00426	8.432	2.865	5.10	0.70	0.95
906.207325	0.01876	5.111	2.408	4.70	0.70	0.53
916.171582	0.83410	1.442	2.670	4.78	0.70	0.78
923.118427*	0.00869	10.22	2.900	5.00	0.70	0.80
970.315022	0.89720	1.920	2.550	4.94	0.64	0.67
987.926764	13.21000	0.258	2.985	4.55	0.68	0.90
1780*	2230	0.952	17.6	30.5	2	5

*Different from MPM89 2

⁺Based on measured data

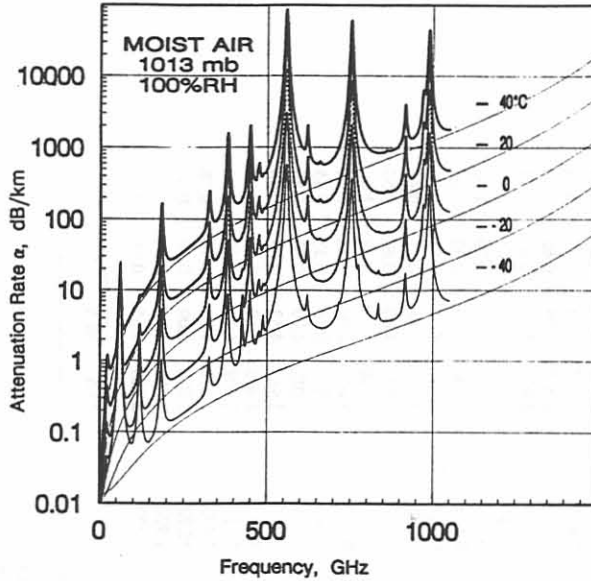


Figure 5. Attenuation α of moist air ($\mu = 100\%$) for frequencies below 1000 GHz at sea-level ($p = 1013$ mb) and temperatures $\pm 40^\circ\text{C}$: — MPM93, Continuum.

Complex permittivity of pure water is expressed by a double-Debye model,²²

$$\epsilon_w = \epsilon_0 - \nu [(\epsilon_0 - \epsilon_1)/(\nu + i\gamma_1) + (\epsilon_1 - \epsilon_2)/(\nu + i\gamma_2)], \quad (9)$$

which provided a best fit to measured ϵ_w data. The static and high-frequency permittivities are

$$\begin{aligned} \epsilon_0 &= 77.66 + 103.3(\theta - 1), \\ \epsilon_1 &= 0.0671 \epsilon_0, \quad \epsilon_2 = 3.52; \end{aligned}$$

and the two relaxation frequencies are

$$\begin{aligned} \gamma_1 &= 20.20 - 146(\theta - 1) + 316(\theta - 1)^2, \\ \gamma_2 &= 39.8 \gamma_1 \text{ GHz}. \end{aligned}$$

The slight temperature dependence of ϵ_2 (reported in Ref. 22) was eliminated to avoid nonphysical behavior for supercooled (-20 to -40°C) water at frequencies above 100 GHz.

A permittivity model for ice was reported by Hufford,²³

$$\epsilon_i = 3.15 + i(a_i/\nu + b_i\nu), \quad (10)$$

where

$$a_i = (\theta - 0.171) \exp(17.0 - 22.1\theta)$$

and

$$b_i = \{[0.233/(1 - 0.993/\theta)]^2 + 6.33/\theta - 1.31\} 10^{-5}.$$

The MPM for fog/cloud cases is $N = N_D + N_V + N_W$. Related attenuation (α) and delay (τ) rates up to 120 GHz are plotted in Fig. 6 for a normalized mass density, $w = 1 \text{ g/m}^3$ (heavy fog, about 50 m visibility) suspended in saturated, sea-level air ($\pm 30^\circ\text{C}$). Below freezing, liquid properties were changed to those of ice. Above freezing one notices that the combined attenuation is almost independent of temperature.

3. RADIO-PATH CHARACTERISTICS

The electromagnetic spectrum between 100 and 1000 GHz is available to expand radio services. This band offers favorable alternatives to both microwave and ir/optical systems. Applications in communication, radar, and remote sensing can profit from larger bandwidth, smaller antenna sizes for a

given spatial resolution, high frequency resolution and, in contrast to ir/optical ranges, a favorable performance under fog/cloud conditions. Besides technical difficulties, the attenuating nature of the earth's atmosphere seriously limits usable path lengths. Except for a few window ranges, the medium at ground levels ($h \leq 1 \text{ km}$) is opaque due to strong absorption lines of water vapor. High mountain sites ($h \leq 4 \text{ km}$), airplanes ($h \leq 15 \text{ km}$), and balloons ($h \leq 35 \text{ km}$) are alternative platforms to escape the water-vapor limitations.

A predictive broadband (1 - 1000 GHz) model for radio characteristics of the neutral atmosphere ($h \leq 130 \text{ km}$) was developed to allow prompt evaluations of the highly variable propagation effects from basic data. Performance of established applications ($\leq 30 \text{ GHz}$) can be translated to (frequency scaling) or combined with new schemes and economical assessments of feasible trade-offs and adaptive measures can be made.

3.1 Transmission and Emission Formulations

Propagation through the nonscattering and nonturbulent inhomogeneous atmosphere is described by the line integral $\int N ds$, where ds is a path differential and the refractivity N was discussed in Sect. 2. Height profiles of N are the basis for calculating delay and loss along the path. Excess delay,

$$D = 3.3356 \int (N_0 + N') ds \text{ ps},$$

is linked to the real part and total path attenuation,

$$A = 0.1820 \nu \int N'' ds \text{ dB}, \quad (11)$$

to the imaginary part.²⁶ The transmission factor,

$$\Gamma = 10^{-0.1 A}, \quad (12)$$

evaluates the energy transfer. A path is said to be opaque when less than 0.1% of the original energy is passed ($\Gamma \leq 0.001$, $A \geq 30 \text{ dB}$). The absorbing atmosphere maintains, up to approximately 90 km height, thermal equilibrium and emits noise radiation at the equivalent blackbody temperature,

$$T_B = 4.191 \times 10^{-2} \nu \int T(s) N''(s) \Gamma(s_0, s) ds \text{ K}. \quad (13)$$

Decreasing transmission leads to increasing emission. The weighting function,

$$W(s) = 4.191 \times 10^{-2} \nu N''(s) \Gamma(s_0, s), \quad (14)$$

determines the height range from where the emission originates. Two cases can be made based on the integration limits for A . In the first one, A is evaluated "upwards", starting at the initial height, h_0 ; secondly, the start is at the final height, h_∞ , and moves "downwards". Reciprocity between path attenuation A_i and brightness $T_{B,i}$ was assumed for polarization-sensitive computations based on the matrix \bar{N} .

3.2 Atmospheric Radio-Path Model

The MPM code (see Sect. 2) is applied in a radio-path model which simulates propagation through an inhomogeneous medium. The atmosphere is spherically stratified in concentric layers between $h = 0$ and 130 km separated by 1-km increments (Δh). Values for $N(h)$ are enumerated by height profiles of $p(h)$, $r(h)$, and $u(h)$. The U.S. Standard Atmosphere and the mid-latitude mean water-vapor profile²⁴ are the defaults of the path model. All computed examples given below are for the default case. It is not difficult to implement different model atmospheres or radiosonde data.

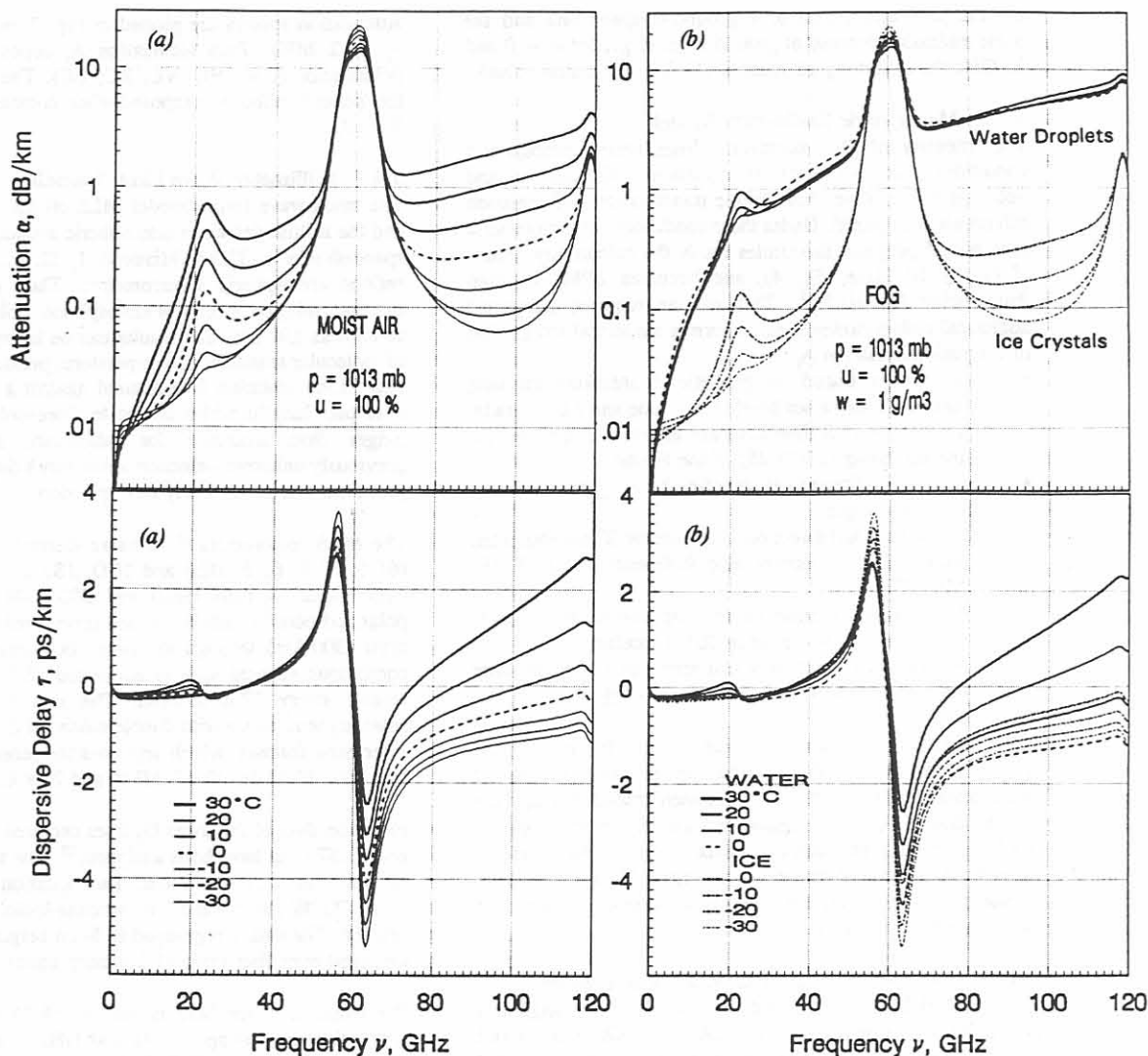


Figure 6. Attenuation rate $\alpha(\nu)$ and delay rate $\tau(\nu)$ up to 120 GHz at temperatures $\pm 30^\circ\text{C}$:
 (a) Moist air at sea-level, $u = 100\%$, (b) water droplets or ice crystals, $w = 1\text{ g/m}^3$, added to (a).

The path differential ds of a slant path is computed by means of the rules of spherical geometry. For elevation angles, $\varphi \geq 10^\circ$, the secant law $ds = \Delta h / \sin \varphi$ follows. In fact, both the curvature of the Earth and refraction determine the path extension of Δh . At very low elevation angles ($\varphi \rightarrow 0$), the height interval Δh is subdivided into $10 \times 0.1\text{-km}$ and further, if needed, into $10 \times 0.01\text{-km}$ groups to approximate more nearly a continuum of N values. When a maximum change of $A_h - A_{h-1} \geq 0.1\text{ dB}$ is detected across an integration layer, the linear interpolation initiates automatically.

The numerical integration of A (Eq. 11) stops at heights h_∞ when increments ΔA become smaller than 0.01 dB (for a limb path after advancing past the tangential height). The path length L is that between h_0 and h_∞ . A numerical integration of T_B (Eq. 13) for emission radiating to the height h_0 follows

$$T_B \approx 0.2303 \sum_h [T(h)(A_h - A_{h-1}) \Gamma(h)] + 2.7 \Gamma(\infty), \quad (15)$$

where $2.7 \Gamma(\infty)$ is the cosmic background term. Superfluous computations are stopped when $W(h) \leq 10^{-6}$. The radio-path model operates at any frequency between 1 and 1000 GHz, and Table 3 summarizes results for 21 and 45 GHz. Listed

TABLE 3.
 Total Attenuation A and Emission T_B at 21 and 45 GHz
 Through a Model Atmosphere.²⁴

Surface values at h_0 : 1013 mb, 15°C , $q = 3.57\text{ g/m}^3$
 ($\int q(h)dh = 10.6\text{ mm}$ for zenith, $\varphi = 90^\circ$)

ν	A	T_B	φ	h_∞	L
GHz	dB	K	deg	km	km
21.0	0.28	19.2	90	11	11
	0.56	34.9	30	13	26
	0.82	48.5	20	15	44
	1.60	85.1	10	17	94
	15.7	274.4	0	26	577
45.0	0.66	39.2	90	17	17
	1.32	71.1	30	19	38
	1.93	96.4	20	22	64
	3.74	154.9	10	21	115
	32.0	285.6	0	31	650

are the path attenuation of a ground-to-space link and the noise emission received at ground level (e.g., for $\varphi = 0$ and 21 GHz the absorbing air mass is 56 times the zenith value).

3.3 Mesospheric Radio-Path Model

The intensity of O_2 microwave lines under mesospheric conditions (≥ 40 km) is location-, direction-, and polarization-sensitive. Anisotropic transmission and emission effects are recognized. Under these conditions the atmospheric path model program substitutes for N the refractivity matrix \bar{N} ($\nu_k \pm 10$ MHz, Eq. 4), and becomes ZPM (Zeeman Propagation Model).^{8, 9} This routine requires numerous additional path parameters to perform a numerical integration of the path attenuation A_i :

- A ray is traced in geodetic coordinates marking altitude h above sea level, LA_titude and LO_ngitude [heights in N-S directions are adjusted to account for the flattening (1/298.25) of the Earth]
- The wave direction is specified by AZ_imuth and elevation angle φ
- Magnitude and direction of the vector B^* are computed using the Int. Geomagnetic Reference Field (IGRF-MAGFIN)²⁵
- Polarization of launched wave or emitted noise power is selected (H/V-Linear or R/L-Circular)
- A frequency range is set in terms of deviation from the selected O_2 line center ($\Delta\nu = \nu_k \pm \nu$).

Two characteristic waves are represented by normalized Stokes parameters and combined to produce the initial polarization.⁸ This combination is then traced through the propagation distance L . Eigenvalues and eigenvectors of the 2×2 plane-wave refractivity matrix are calculated for the orientation angle ϕ between wave vector E^* and magnetic vector B^* . The propagating field is a linear combination of two characteristic waves.

Individual integration steps of ZPM at the line center, $\nu_k = 61.150$ GHz, are detailed in Table 4: A ray originates at the 300-km orbital height (h , LA, LO, AZ, and φ) and passes through the atmosphere to a minimum, tangential height, $h_t = 90$ km.

Attenuation spectra are plotted in Fig. 7 over the range, $\nu_k \pm 2$ MHz. Path attenuation A_i depends on the initial polarization ($i = HL, VL, RC, LC$). The main features of the Zeeman effect are exposed when compared with the case $B = 0$.

3.4 Millimeter-Wave Limb Sounding

The microwave limb sounder MLS on the UARS satellite²⁶ and the millimeter-wave atmospheric sounder MAS²⁷ on the space-shuttle (ATLAS Missions I, II, ...) both are very refined atmospheric spectrometers. They measure globally thermal emission spectra of atmospheric molecules at altitudes as high as 150 km. The results can be interpreted in profiles of molecular abundances, temperature, pressure, and magnetic field. Line emission is measured against a 3 K background over path lengths which are up to three-orders of magnitude longer than available for laboratory spectroscopy. A previously unknown detection sensitivity brings answers to old problems and raises many new questions.

The MAS radiometers²⁷ measure thermal emission from O_2 (61.1, 63.0, 63.6 GHz) and H_2O (183 GHz), and from the trace gases O_3 (184 GHz) and ClO (204 GHz). An HL-polarized pencil-beam is scanned downwards from the shuttle orbit (300 km) through the limb. In normal operation, the continuous vertical scan is calibrated (2.7 and 300 K) and repeats every 12.8 seconds. The radiometers are super-heterodyne receivers with double-sideband (DSB) detection. A filter bank follows, which separates the received noise power into 10×40 -MHz, 20×2 -MHz, and 20×0.2 -MHz outputs.

Emission data of the three O_2 lines centered at 61.15, 63.00, and 63.57 GHz have been analyzed.²⁸ The tangential heights ranged from 125 to 10 km. Two locations were selected: $70^\circ N, 70^\circ W$ (shuttle at $57^\circ N$, antenna looks north) and at the equator. The data are grouped in 5-km height increments and averaged over five scans (1.2 s integration).

The example given here is for the 61.150 GHz line. The upper sideband (image) at 71.630 GHz responds to cosmic background radiation (2.7 K). The measured mean is to first order about half the theoretical single sideband level.

TABLE 4.
Path Attenuation $A_i(h)$ and Noise Emission $T_{B,i}$ for a Limb Path ($h_t = 90$ km) at $\nu_o = 61.15056$ GHz.
Antenna is located at $57^\circ N/70^\circ W$, $h = 300$ km and looks down ($\varphi = -14.57^\circ$) towards north (AZ = 0°) to receive linear-polarized radiation (results for $i = VL-, RC-$ and $LC-$ polarizations are also given).

h	LA	LO	AZ	φ	B	ϕ	L	A_{HL}	A_{VL}	W_{HL}	W_{VL}	A_{RC}	A_{LC}
km	deg	deg	deg	deg	μT	deg	km	dB		km^{-1}		dB	
300	57.0	-70	0	-14.57			0	$T_B(DFS) = 67.8$ K (ZPM)			63 ± 2 K (MAS)		
↓							↓	$T_B(SSB) = 131.2$			174.5	153.0	153.0 K
129	65.2	-70	0	-6.39	55.1	78.4	954	0.00	0.00	.000	.000	0.00	0.00
↓							↓			↑			
91	70.4	-70	0	-1.14	55.4	85.6	1548	1.30	2.92	.060	.094	2.03	2.03
90	71.0	-70	0	-0.53	55.4	86.2	1616	1.97	4.45	.099	.126	3.04	3.04
91	72.1	-70	0	0.53	55.3	87.3	1736	3.39	7.66	.150	.127	5.02	5.02
92	72.7	-70	0	1.14	55.2	88.4	1805	4.06	9.20	.061	.042	5.91	5.91
↓							↓						
129	77.7	-70	0	6.15	53.7	94.9	2371	5.15	11.68	.000	.000	7.29	7.29
130	77.8	-70	0	6.23	53.7	95.0	2380	5.15	11.68	.000	.000	7.29	7.29

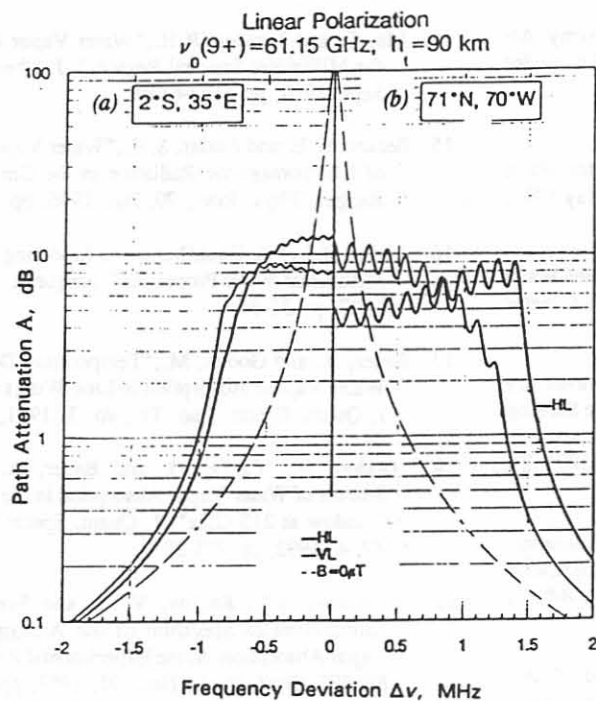


Figure 7. Spectra ($\nu_0 \pm 2 \text{ MHz}$) of total attenuations A_i ($i = \text{HL, VL}$) and A_0 ($B = 0$) for a limb path ($h_t = 90 \text{ km}$) through the U.S. Std. Atmos. ²⁴ at two locations marked (a) and (b).

The data are shown in Fig. 8 and serve as a test case for ZPM predictions.^{24, 25} Limb-emission was measured for tangential heights ranging from 30 to 120 km at the northern location 71°N/70°W. Table 4 lists the variables that enter a computation of $T_B(\nu_k)$. Very height-selective ($\Delta h \leq 1 \text{ km}$) temperature sounding between 115 and 80 km is indicated by the weighting function $W(h)$, Eq. (14). At $h_t = 78 \text{ km}$, the path abruptly becomes opaque and T_B assumes about half the physical temperature of the 78-km level (98 K). Below $h_t = 40 \text{ km}$, the upper sideband at 71.63 GHz "warms up" due to absorption by water vapor and dry air, which is computed by means of MPM.

4. CONCLUSIONS

Propagation characteristics of the atmosphere are predicted by the general refractivity N , and for Zeeman-broadening by the special refractivity matrix \tilde{N} . Transmission and emission properties of the inhomogeneous atmosphere (e.g., excess path delay, total attenuation, opacity, sky noise, etc.) were modeled from known path profiles of physical variables.

The new code MPM93 reproduces the spectral characteristics of the clear atmosphere (O_2 , H_2O) between 18 and 930 GHz within the uncertainty limits of five reported controlled experiments.^{15 - 19}

ZPM reproduces the main features of measured thermal radiation signatures stemming from Zeeman-split oxygen lines. The solution to the forward-transfer problem^{8, 9, 28} can serve as a starting point to develop profile inversion algorithms.^{7, 13} Validation, error checking of predictions, and incorporation of new research results will continue to be critical and time consuming tasks in the effort to refine understanding and modeling of electromagnetic wave propagation through the neutral atmosphere.

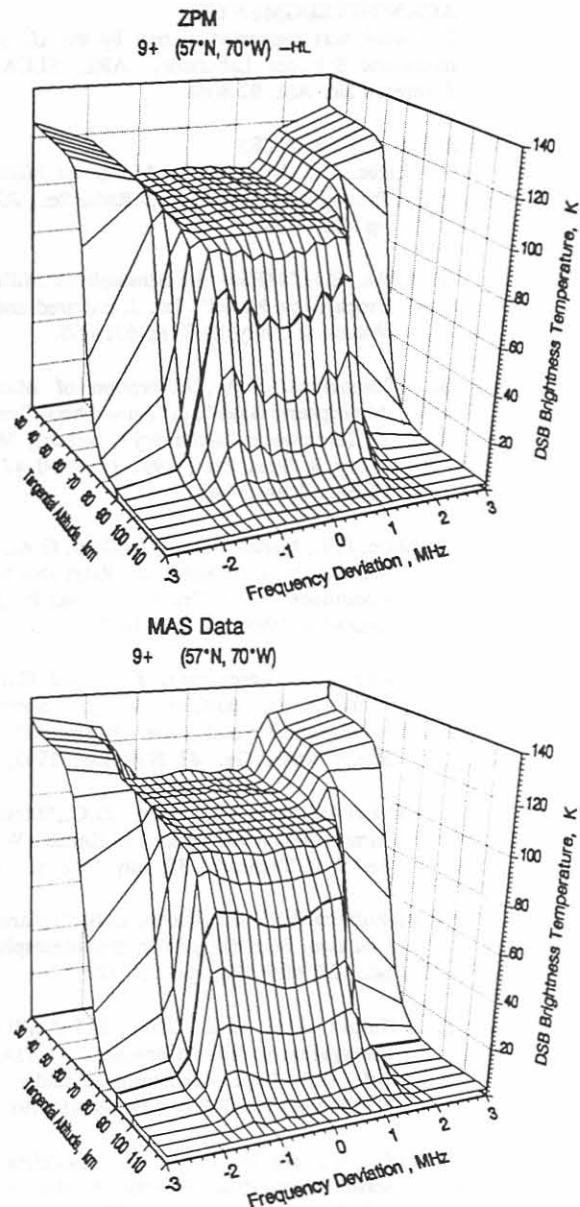


Figure 8. DSB-emission of the 9^+ line ($\nu_k \pm 3 \text{ MHz}$) from a limb scan, $h_t = 30$ to 120 km , approximately centered over $70^\circ\text{N}, 70^\circ\text{W}$: (a) ZPM predictions for HL polarization and (b) MAS data^{**}.

^{**} The MAS-project was supported by the German agencies BMFT and DARA under FKZ 50 QS 8502, 9002, by NASA, and by the MAS-PI agencies: MPAA (Katlenburg-Lindau, FRG); NRL (Washington, D.C., USA); IAP (Berne, CH); and IfE (Bremen, FRG).

ACKNOWLEDGMENTS

The work was supported in part by the U. S. Army Atmospheric Sciences Laboratory, ARL, SLCAS-BA under Reference No. ASL 92-8058.

5. REFERENCES

1. Liebe, H.J., "An Updated Model for Millimeter Wave Propagation in Moist Air," *Radio Sci.*, 20, May 1985, pp 1069-1089.
2. Liebe, H.J., "MPM - An Atmospheric Millimeter-Wave Propagation Model", *Int. J. Infrared and Millimeter Waves*, 10, July 1989, pp 631-650.
3. Rosenkranz, P.W., "Absorption of Microwaves by Atmospheric Gases", in "Atmospheric Remote Sensing By Microwave Radiometry"; Janssen, M.A., ed.; J. Wiley & Sons, Inc., 1993 (ISBN 0 471 62891 3), Chapter 2, pp 37-90.
4. Liebe, H.J., Manabe, T. and Hufford, G.A., "Millimeter-Wave Attenuation and Delay Rates Due to Fog/Cloud Conditions", *IEEE Trans. Antennas Propag.*, AP-37, December 1989, pp 1617-1623.
5. Liebe, H.J., Rosenkranz, P.W. and Hufford, G.A., "Atmospheric 60-GHz Oxygen Spectrum: New Measurements and Line Parameters", *J. Quant. Spectr. Radiat. Tr.*, 48, Nov./Dec. 1992, pp 629-643.
6. Crawford, A.B. and Hogg, D.C., "Measurement of Atmospheric Attenuation at Millimeter Wavelengths", *Bell Syst. Techn. J.*, 35, July 1956, pp. 907-916.
7. Rosenkranz P.W. and Staelin, D.H., "Polarized Thermal Emission from Oxygen in the Mesosphere", *Radio Sci.*, 23, May 1988, pp 721-729.
8. Hufford G.A. and Liebe, H.J., "Millimeter-Wave Propagation In The Mesosphere", NTIA-Report 89-249, U.S. Dept. Commerce, Boulder, CO, 1989; NTIS Order No. PB 90-119868/AF (1989).
9. Liebe, H.J. and Hufford, G.A., "Modeling Millimeter-wave Propagation Effects in the Atmosphere", AGARD CP-454, October 1989, Paper 18.
10. Goff, J.A. and Gratch, S., "Low-Pressure Properties of Water from -160 to 212°F", *Trans. Amer. Soc. Heat. Vent. Eng.*, 52, 1946, pp 95-121 (also see List, R.J., "Smithsonian Meteorological Tables", Washington D.C., Smithsonian Inst., 1966).
11. Bauer, A., Godon, M., Kheddar, M. and Hartmann, J.M., "Temperature and Perturber Dependences of Water Vapor Line-Broadening: Experiments at 183 GHz, Calculations Below 1000 GHz", *J. Quant. Spectr. Radiat. Tr.*, 41, 1, 1989, pp 49-54.
12. Poynter, R.L., Pickett, H.M., and Cohen, E., "Submillimeter, Millimeter, and Microwave Spectral Line Catalogue", JPL Publication 80-23, Revision 3, 1991, NASA-JPL, Pasadena, CA.
13. Westwater, Ed.R., "Groundbased Microwave Radiometry", in "Atmospheric Remote Sensing By Microwave Radiometry", Janssen, M.A., ed.; J. Wiley & Sons, Inc., 1993 (ISBN 0 4710 62891 3), pp 145-213.
14. Ma, Q. and Tipping, R.H., "Water Vapor Continuum in the Millimeter Spectral Region", *J. Chem. Phys.*, 93, Sept. 1990, pp 6127-6139.
15. Becker, G.E. and Autler, S.H., "Water Vapor Absorption of Electromagnetic Radiation in the Cm Wave-length Range", *Phys. Rev.*, 70, Jan. 1946, pp 300-307.
16. Liebe, H.J., "A Contribution to Modeling Atmospheric Millimeter-Wave Properties", *Frequenz*, 41, Jan./Feb. 1987, pp 31-36.
17. Bauer, A. and Godon, M., "Temperature Dependence of Water Vapour Absorption in Line-Wings at 190 GHz", *J. Quant. Spectr. Radi. Tr.*, 46, 3, 1991, pp 211-220.
18. Godon, M., Carlier, J. and Bauer, A., "Laboratory Studies of Water Vapor Absorption in the Atmospheric Window at 213 GHz", *J. Quant. Spectr. Radiat. Tr.*, 47, 4, 1992, pp 275-285.
19. Furashov, N.I., Katkov, V.Yu. and Svertlov, B.A., "Submillimetre Spectrum of the Atmospheric Water Vapor Absorption- Some Experimental Results", *ICAP 89, IEE Conf. Publ.*, No. 301, 1989, pp 310-311.
20. Hill, R.J., "Dispersion by Atmospheric Water Vapor at Frequencies Less Than 1 THz", *IEEE Trans. Antennas Propag.*, AP-36, 3, March 1988, pp 423-430.
21. Rosenkranz, P.W., "Pressure Broadening of Rotational Bands.II. Water Vapor from 300 to 1100 cm⁻¹", *J. Chem. Phys.*, 87, July 1987, pp 163-170.
22. Liebe, H.J., Hufford, G.A. and Manabe, T., "A Model for the Complex Permittivity of Water at Frequencies Below 1 THz", *Int. J. Infrared and Millimeter Waves*, 12, July 1991, pp 659-675.
23. Hufford, G.A., "A Model for the Complex Permittivity of Ice at Frequencies Below 1 THz", *Int. J. Infrared and Millimeter Waves*, 12, July 1991, pp 677-680.
24. COESA, U.S. Committee on Extension to the Standard Atmosphere, "U.S. Standard Atmosphere 76", NOAA-S/T 76-1562; U.S. Gov. Printing Office, Washington, D.C., 1976.
25. Barraclough, D.R., "International Geomagnetic Reference Field revision 1985", *Pure and Appl. Geophys.*, 123, 1985, pp 641-645.
26. Waters, J.W., "Microwave Limb Sounding", in "Atmospheric Remote Sensing By Microwave Radiometry", Janssen, M.A., ed.; J. Wiley & Sons, Inc., 1993 (ISBN 0 4710 62891 3), Chapter 8, pp 383-496.
27. Croskey, C.L. et al., "The Millimeter Wave Atmospheric Sounder (MAS): A Shuttle-Based Remote Sensing Experiment", *IEEE Trans. Microw. Theory and Techniques*, MTT-40, June 1992, pp 1090-1099.
28. Cotton, M.G., Degenhardt, W., Hartmann, G.K., Hufford, G.A., Liebe, H.J., and Zwick, R., "Analysis of MAS Emission Signatures from three O₂ Microwave Lines", NTIA Report 93-000, in review, 1993.

AGARD holds limited quantities of the publications that accompanied Lecture Series and Special Courses held in 1993 or later, and of AGARDographs and Working Group reports published from 1993 onward. For details, write or send a telefax to the address given above. *Please do not telephone.*

AGARD does not hold stocks of publications that accompanied earlier Lecture Series or Courses or of any other publications. Initial distribution of all AGARD publications is made to NATO nations through the National Distribution Centres listed below. Further copies are sometimes available from these centres (except in the United States). If you have a need to receive all AGARD publications, or just those relating to one or more specific AGARD Panels, they may be willing to include you (or your organisation) on their distribution list. AGARD publications may be purchased from the Sales Agencies listed below, in photocopy or microfiche form.

NATIONAL DISTRIBUTION CENTRES

BELGIUM

Coordonnateur AGARD — VSL
Etat-Major de la Force Aérienne
Quartier Reine Elisabeth
Rue d'Evere, 1140 Bruxelles

CANADA

Director Scientific Information Services
Dept of National Defence
Ottawa, Ontario K1A 0K2

DENMARK

Danish Defence Research Establishment
Ryvangs Allé 1
P.O. Box 2715
DK-2100 Copenhagen Ø

FRANCE

O.N.E.R.A. (Direction)
29 Avenue de la Division Leclerc
92322 Châtillon Cedex

GERMANY

Fachinformationszentrum
Karlsruhe
D-7514 Eggenstein-Leopoldshafen 2

GREECE

Hellenic Air Force
Air War College
Scientific and Technical Library
Dekelia Air Force Base
Dekelia, Athens TGA 1010

ICELAND

Director of Aviation
c/o Flugrad
Reykjavik

ITALY

Aeronautica Militare
Ufficio del Delegato Nazionale all'AGARD
Aeroporto Pratica di Mare
00040 Pomezia (Roma)

LUXEMBOURG

See Belgium

NETHERLANDS

Netherlands Delegation to AGARD
National Aerospace Laboratory, NLR
P.O. Box 90502
1006 BM Amsterdam

NORWAY

Norwegian Defence Research Establishment
Attn: Biblioteket
P.O. Box 25
N-2007 Kjeller

PORTUGAL

Força Aérea Portuguesa
Centro de Documentação e Informação
Alfragide
2700 Amadora

SPAIN

INTA (AGARD Publications)
Pintor Rosales 34
28008 Madrid

TURKEY

Milli Savunma Başkanlığı (MSB)
ARGE Daire Başkanlığı (ARGE)
Ankara

UNITED KINGDOM

Defence Research Information Centre
Kentigern House
65 Brown Street
Glasgow G2 8EX

UNITED STATES

National Aeronautics and Space Administration (NASA)
Langley Research Center
M/S 180
Hampton, Virginia 23665

The United States National Distribution Centre (NASA/Langley) does NOT hold stocks of AGARD publications. Applications for copies should be made direct to the NASA Center for Aerospace Information (CASI) at the address below.

SALES AGENCIES

NASA Center for
Aerospace Information (CASI)
800 Elkridge Landing Road
Linthicum Heights, MD 21090-2934
United States

ESA/Information Retrieval Service
European Space Agency
10, rue Mario Nikis
75015 Paris
France

The British Library
Document Supply Centre
Boston Spa, Wetherby
West Yorkshire LS23 7BQ
United Kingdom

Requests for microfiches or photocopies of AGARD documents (including requests to CASI) should include the word 'AGARD' and the AGARD serial number (for example AGARD-AG-315). Collateral information such as title and publication date is desirable. Note that AGARD Reports and Advisory Reports should be specified as AGARD-R-*nnn* and AGARD-AR-*nnn*, respectively. Full bibliographical references and abstracts of AGARD publications are given in the following journals:

Scientific and Technical Aerospace Reports (STAR)
published by NASA Scientific and Technical
Information Program
NASA Headquarters (JTT)
Washington D.C. 20546
United States

Government Reports Announcements and Index (GRA&I)
published by the National Technical Information Service
Springfield
Virginia 22161
United States
(also available online in the NTIS Bibliographic
Database or on CD-ROM)



Printed by Specialised Printing Services Limited
40 Chigwell Lane, Loughton, Essex IG10 3TZ